A minimal model for two-component FIMP dark matter:
A basic search

S. Peyman Zakeri[1]   S. Mohammad Moosavi Nejad[1,2]   Mohammadreza Zakeri[3,4]   S. Yaser Ayazi[5]

[1] Faculty of Physics, Yazd University, Yazd, Iran
[2] School of Particles and Accelerators, Institute for Research in Fundamental Sciences (IPM), Tehran, Iran
[3] Physics and Astronomy Department, University of California, California 92521, USA
[4] CAS Key Laboratory of Theoretical Physics, Institute of Theoretical Physics, Chinese Academy of Sciences, Beijing 100190, China
[5] Physics Department, Semnan University, Semnan, Iran

Abstract: In the multi-component configurations of dark matter phenomenology, we propose a minimal two-component configuration which is an extension of the Standard Model with only three new fields; one scalar and one fermion interact with the thermal soup through Higgs portal, mediated by the other scalar in such a way that the stabilities of dark matter candidates are made simultaneously by an explicit Z_2 symmetry. Against the most common freeze-out framework, we look for dark matter particle signatures in the freeze-in scenario by evaluating the relic density and detection signals. A simple distinguishing feature of the model is the lack of dark matter conversion, so the dark matter components act individually and the model can be adapted entirely to both singlet scalar and singlet fermionic models, separately. We find dark matter self-interaction as the most promising approach to probe such feeble models. Although the scalar component satisfies this constraint, the fermionic one refuses it even in the resonant region.

1   Introduction

Weakly interacting massive particles (WIMPs) are the most popular solution to the puzzle of dark matter (DM) [1–3]. In TeV scale (LHC scale) new physics, DM particles follow the thermal scenario in which they reach thermal and chemical equilibrium with the bath particles but lose it at the freeze-out temperature (which is around $m_{\rm DM}/20$) and experience decoupling from the Universe plasma. WIMP candidates such as the neutralino [4] and Kaluza-Klein particle [5, 6] are found in theories such as the minimal supersymmetric Standard Model (MSSM) and universal extra dimensions (UED), respectively, and also in other extensions of the Standard Model (SM) such as singlet scalar [7–10] (or fermionic [11–13]) DM. In spite of their popularity, WIMPs have not yet been detected in direct experiments.

The other viable and well-motivated hypothesis to explain the DM problem is that there is such a feeble interaction that DM particles can never be abundant enough to thermalize. In this so-called freeze-in mechanism [14–16], feebly interacting massive particles (FIMPs) have been slowly produced in the early Universe through the collisions or decays of the bath particles. FIMP candidates are motivated in various extensions of the SM [17–19] and a well-known example which arises from neutrino physics is the sterile neutrino [20–24]. It is difficult to detect FIMP particles because of their small couplings with the SM. As for the indirect searches, depending on the type of DM candidate, i.e. scalar [25], fermion [19], etc, some experiments have parameter space where they could survive but these are very borderline. For a study of the non-thermal properties of dark matter see Ref. [26].

Although a lot of attention has been dedicated to single-particle DM models, some studies have considered DM models with the contribution of more particles in the observed DM density (multi-component DM [27–31]). The simplest and the most common case is the union of the singlet scalar (fermionic) and the singlet fermionic (scalar) models which are employed in both freeze-in [25, 32] and freeze-out [33–36] solutions (or intermediate cases [37]). Nevertheless, it remains a mystery whether DM is a single particle or multi-component.

In this paper, we analyze whether the freeze-in approach can be properly used to produce the observed

DM density in our Universe. We choose a minimal two-component DM model in such a way that both of the components are FIMP particles. Following our hypothesis, we consider a singlet scalar and a Dirac fermion where an accidental symmetry guarantees their stabilities and a Higgs portal enables them to interact with the SM particles. The most striking feature of our model is its simplicity, as the two candidates of DM particles do not couple with each other and the model has separate overlaps with both the singlet scalar model [17] and the singlet fermionic model [18]. In our work, all contributing processes to the relic density are assumed and supplementary phenomenological aspects are also included.

Some promising possible signatures of FIMPs which are found to be most reliable in previous works are the γ-ray excess observed from the Galactic center (GC) [32, 37], the X-ray line at 3.55 keV [32, 37], and DM self-interaction [25, 37]. To generate the gamma ray excess, the fermionic component should have a pseudoscalar coupling to the mediator in the freeze-out regime [37]. The scalar component which does also couple to the SM Higgs directly [32], should not feature large valued couplings. An X-ray signal with $E_\gamma = 3.55$ keV from the XMM-Newton telescope and a similar signal at 3.52 keV from the Andromeda galaxy (M31) and Perseus Cluster could all be interpreted by the decay [38] or the annihilation [39] of DM. However, this requires a definite decay rate and annihilation cross section which is out of reach for our scenario. Therefore, we continue our probe relying only on the DM self-interaction. This non-gravitational interaction is a well-motivated indirect search as it solves the tensions between observations and simulations of the small-scale structure of DM.

Following the aforementioned setup, our paper is organized as follows. After introducing the construction of our model and identifying its parameter space in Section 2, we solve two independent Boltzmann equations in the following section (Section 3), in order to reach the observed relic density measured by the WMAP and Planck experiments [40]. In Section 4, we study the phenomenological implications for both direct and indirect experiments, and summarize our results in Section 5.

2   Two-component FIMP DM

Beyond the SM, we employ three new fields to furnish our model: two scalars (χ and S) and one Dirac fermion (ψ), which are all assumed to be singlet under the SM gauge groups. A discrete Z_2 symmetry is applied such that it reads the SM fields and the S-scalar even, and the other two fields (χ and ψ) odd. This symmetry guarantees the stability of both odd particles in a way that we do not have any terms involving both fields ψ and χ. In this way, the decays of odd particles to one

another are prevented. Therefore, we can have two DM candidates in our setup by an accidental symmetry. The framework of our model is constructed by:

$$\mathcal{L} \supset \frac{1}{2}(\partial_\mu S)^2 + \frac{1}{2}(\partial_\mu \chi)^2 + i\bar{\psi}\slashed{\partial}\psi$$
$$- m_\psi \bar{\psi}\psi - g_s S\bar{\psi}\psi - g_p S\bar{\psi}\gamma^5\psi$$
$$- V(H,S,\chi), \tag{1}$$

where we introduced the scalar and pseudoscalar interactions with the couplings g_s and g_p, respectively, and inserted the scalar interactions in the term $V(H,S,\chi)$ as

$$V(H,S,\chi) = -\mu_H^2 H^\dagger H + \lambda_H (H^\dagger H)^2 + \mu_1 S + \frac{1}{2}\mu_S^2 S^2$$
$$+ \frac{1}{3!}\alpha_s S^3 + \frac{1}{4!}\lambda_S S^4 + \frac{1}{2}m_{0\chi}^2 \chi^2 + \frac{1}{4!}\lambda_\chi \chi^4$$
$$+ \lambda_1 S H^\dagger H + \lambda_2 S^2 H^\dagger H + \lambda_{\chi H}\chi^2 H^\dagger H$$
$$+ \lambda_3 S\chi^2 + \lambda_4 S^2 \chi^2. \tag{2}$$

After spontaneous symmetry breaking, the $SU(2)$ Higgs doublet is parametrized as

$$H = \frac{1}{\sqrt{2}}\begin{pmatrix} 0 \\ v_H + h \end{pmatrix}, \tag{3}$$

where $v_H = 246$ GeV, but for the mediator we assume that it does not acquire a vacuum expectation value, i.e. $<S> = 0$, which minimalizes our model too. Now, due to the interaction terms in Eq. (2), h and S mix with each other and form a mass matrix with the following eigenstates

$$h_1 = S\sin\theta + h\cos\theta,$$
$$h_2 = S\cos\theta - h\sin\theta, \tag{4}$$

and the eigenvalues as

$$m_{h_1,h_2}^2 = \frac{m_h^2 + m_S^2}{2} \pm \frac{m_h^2 - m_S^2}{2}\sqrt{1+y^2}, \quad \text{with} \quad y = \frac{2m_{h,S}^2}{m_h^2 - m_S^2}, \tag{5}$$

where θ is the mixing angle between h_1 and h_2 such that

$$\tan\theta = \frac{y}{1+\sqrt{1+y^2}}. \tag{6}$$

According to the definition of the mixing angle θ, h_1 can be considered as the SM-like Higgs observed at the LHC with a mass of about 125 GeV. In Eq. (5), $m_h = \sqrt{2\lambda_H}v_H$, $m_S = (\lambda_2 v_H^2 + \mu_S^2)^{1/2}$ and $m_{h,S} = \sqrt{\lambda_1}v_H$.

Concerning our parameters, vacuum stability implies that the scalar potential in Eq. (2) must be bounded from below. On the other hand, perturbativity does not allow the model parameters to be too large. Eventually, these theoretical conditions can be satisfied if one has

$$-2\pi/3 < \lambda_S, \lambda_\chi < 2\pi/3,$$
$$-4\pi < \lambda_2, \lambda_{\chi H} < 4\pi,$$

$$-8\pi<\lambda_4,g_s,g_p<8\pi,$$
$$\lambda_2+\sqrt{\lambda_H\lambda_S}>0,$$
$$\lambda_{\chi H}+\sqrt{\lambda_H\lambda_\chi}>0,$$
$$2\lambda_4+\sqrt{\lambda_S\lambda_\chi}>0, \tag{7}$$

and

$$\left(\sqrt{2(\lambda_2+\sqrt{\lambda_H\lambda_S})(\lambda_{\chi H}+\sqrt{\lambda_H\lambda_\chi})(2\lambda_4+\sqrt{\lambda_S\lambda_\chi})}\right.$$
$$\left.+\sqrt{\lambda_H\lambda_S\lambda_\chi}+\lambda_2\sqrt{\lambda_\chi}+\lambda_{\chi H}\sqrt{\lambda_S}+2\lambda_4\sqrt{\lambda_H}\right)>0, \tag{8}$$

where λ_H is the quartic coupling of H. Extending the SM with the new fields ψ, χ and S embeds 19 parameters in addition to the SM ones. They are $m_S,m_\chi,m_\psi,g_s,g_p,\mu_1,\alpha_S,\lambda_S,\lambda_\chi,\lambda_1,\lambda_2,\lambda_{\chi H},\lambda_3,\lambda_4,m_{h_1},m_{h_2}$, $\sin\theta,v_H$, and m_h. However, due to the 8 model constraints, 11 independent parameters,

$$g_s,\ g_p,\ \lambda_3,\ \lambda_4,\ \lambda_{\chi H},\ m_\psi,\ m_\chi,\ m_{h_2},\ \sin\theta, \tag{9}$$

remain for the relic abundance and for indirect searches, λ_H and λ_χ are required. Here, we take a moment to describe the eight constraints which appear in our work. Note that, after spontaneous symmetry breaking the scalar potential given in Eq. (2) reads as $V(h,S,\chi)$. Therefore, it can be deduced from the potential that:

$$1)\quad \left.\frac{\partial V}{\partial h}\right|_{h=S=\chi=0}=0\Rightarrow\mu_H^2=\lambda_H v_H^2, \tag{10}$$

$$2)\quad \left.\frac{\partial V}{\partial S}\right|_{h=S=\chi=0}=0\Rightarrow\mu_1=-\frac{\lambda_1 v_H^2}{2}, \tag{11}$$

$$3)\quad m_h^2=-\mu_H^2+3\lambda_H v_H^2=2\lambda_H v_H^2, \tag{12}$$

$$4)\quad m_S^2=\mu_S^2+\lambda_2 v_H^2, \tag{13}$$

$$5)\quad m_\chi^2=m_{0\chi}^2+\lambda_{\chi H}v_H^2. \tag{14}$$

Also, the mixing between S and h produces the scalars h_1 and h_2 so one can conclude that

$$\frac{1}{2}m_h^2 h^2+\frac{1}{2}m_S^2 S^2+\lambda_1 v_H Sh=\frac{1}{2}m_{h_1}^2 h_1^2+\frac{1}{2}m_{h_2}^2 h_2^2. \tag{15}$$

Substituting $h_1=S\sin\theta+h\cos\theta$ and $h_2=S\cos\theta-h\sin\theta$ (4) and using the constraints (3)–(5), one obtains:

$$6)\quad \lambda_H=\frac{m_{h_1}^2\cos^2\theta+m_{h_2}^2\sin^2\theta}{2v_H^2}, \tag{16}$$

$$7)\quad \lambda_2=\frac{m_{h_1}^2\sin^2\theta+m_{h_2}^2\cos^2\theta-\mu_S^2}{v_H^2}, \tag{17}$$

$$8)\quad \lambda_1=\frac{m_{h_1}^2-m_{h_2}^2}{2v_H}\sin2\theta. \tag{18}$$

These 8 constraints reduce the 19 free parameters in the model to the 11 independent parameters. Also, the couplings α_s and λ_2 can be taken as zero without any ambiguities. However, we consider $\alpha_s\neq0$ for future applications. In the following, we will probe our model parameter space with experimental constraints coming from the relic density, direct and indirect detections.

3 DM Density

3.1 Boltzmann Equation

Since our model contains two DM candidates, its relic density has contributions from both fields ψ and χ. Therefore, we have to solve two Boltzmann equations for particles which will not reach equilibrium in the freeze-in mechanism where we follow the solution in Ref. [19] (following Ref. [15]). The time evolution of number density, $dn_{\rm DM}/dt$, for the fermionic DM is given by

$$\frac{dn_\psi}{dt}+3Hn_\psi=\frac{T}{\pi^2}\sum_{i=1}^2 m_{h_i}^2 K_1\left(\frac{m_{h_i}}{T}\right)\Gamma_{h_i\to\bar\psi\psi}+\frac{T}{32\pi^4}\sum_{j=f,Z,W,h_1,h_2}\int_{4m_j^2}^\infty ds\,\sigma_{jj\to\bar\psi\psi}(s)(s-4m_j^2)\sqrt{s}K_1\left(\frac{\sqrt{s}}{T}\right), \tag{19}$$

and for the scalar DM, it reads

$$\frac{dn_\chi}{dt}+3Hn_\chi=\frac{T}{\pi^2}\sum_{i=1}^2 m_{h_i}^2 K_1\left(\frac{m_{h_i}}{T}\right)\Gamma_{h_i\to\chi\chi}+\frac{T}{32\pi^4}\sum_{j=f,Z,W,h_1,h_2}\int_{4m_j^2}^\infty ds\,\sigma_{jj\to\chi\chi}(s)(s-4m_j^2)\sqrt{s}K_1\left(\frac{\sqrt{s}}{T}\right). \tag{20}$$

Here H is the Hubble constant, K_1 is the modified Bessel function of order 1 and s is the center of mass energy squared. All contributions to the DM relic density are considered in the corresponding cross sections and decay widths in the two above equations. Our analytical results for the cross sections and decay widths are presented in the Appendix. The number density of DM particles is calculated as $n_i=\frac{g_i}{(2\pi)^3}\int d^3p f_i$ [16, 41, 42] (with $i=\psi,\chi$), where f_i is the phase space density of particle

i with the g_i-internal spin degrees of freedom. As it is well-known from the freeze-in mechanism of production, the two DM candidates in the present model have negligible initial abundance (individually), thus we may set $f_i=0$. Consequently, it can be derived from Eqs. (19) and (20) that the process of DM conversion, i.e. $\chi\chi\leftrightarrow\bar\psi\psi$, does not contribute to the total relic abundance and is suppressed in our next calculations. On the other hand, each of the DM candidates, independent of the other, can be produced or annihilated in the Universe.

By solving Eqs. (19) and (20), one can obtain the number densities (n_ψ, n_χ) scaled to the entropy of Universe $\hat{s}$, i.e. $Y_\psi = n_\psi/\hat{s}$ and $Y_\chi = n_\chi/\hat{s}$, as

$$
Y_\psi = \frac{1}{4\pi^4} \frac{45 M_{pl}}{1.66 g_s^*(T)\sqrt{g_\rho^*}} \left[2\sum_{i=1}^{2} \Gamma_{h_i\to\bar\psi\psi} m_{h_i}^2 \int_{T_{\mathrm{Now}}}^{\infty} \mathrm{d}T \frac{K_1\left(\frac{m_{h_i}}{T}\right)}{T^5} \right.
$$
$$
\left. + \sum_{j=f,Z,W,h_1,h_2} \frac{1}{16\pi^2} \int_{T_{\mathrm{Now}}}^{\infty} \mathrm{d}T \frac{1}{T^5} \int_{4m_j^2}^{\infty} \mathrm{d}s\, \sigma_{jj\to\bar\psi\psi}(s)(s-4m_j^2)\sqrt{s} K_1\left(\frac{\sqrt{s}}{T}\right) \right], \tag{21}
$$

and

$$
Y_\chi = \frac{1}{4\pi^4} \frac{45 M_{pl}}{1.66 g_s^*(T)\sqrt{g_\rho^*}} \left[2\sum_{i=1}^{2} \Gamma_{h_i\to\chi\chi} m_{h_i}^2 \int_{T_{\mathrm{Now}}}^{\infty} \mathrm{d}T \frac{K_1\left(\frac{m_{h_i}}{T}\right)}{T^5} \right.
$$
$$
\left. + \sum_{j=f,Z,W,h_1,h_2} \frac{1}{16\pi^2} \int_{T_{\mathrm{Now}}}^{\infty} \mathrm{d}T \frac{1}{T^5} \int_{4m_j^2}^{\infty} \mathrm{d}s\, \sigma_{jj\to\chi\chi}(s)(s-4m_j^2)\sqrt{s} K_1\left(\frac{\sqrt{s}}{T}\right) \right], \tag{22}
$$

where M_{pl} is the Planck mass, and g_s^* and g_ρ^* are the effective numbers of degrees of freedom.

3.2   Relic Abundance

The most important constraint which should be satisfied in models describing DM is the observed relic density. As the Planck experiments have measured the current amount of DM [40], our first experimental constraint is described as

$$
\Omega_{\mathrm{DM}}h^2 = \Omega_\psi h^2 + \Omega_\chi h^2 = 0.1199 \pm 0.0027, \tag{23}
$$

where h is the Hubble parameter scaled in units of 100 km/s.Mpc. Using the yield calculated in the previous section (Eqs. (21) and (22)), we can obtain the relic density as

$$
\Omega_i h^2 = 2.742\times10^{-8}\left(\frac{m_i}{\mathrm{GeV}}\right)Y_i(T_0), \quad i=\psi,\chi. \tag{24}
$$

First, we start with the scalar component of the model. The dependence of DM density is evaluated over the relevant parameters. The predicted relic density of our model is best behaved at $m_{h_2}=100$ GeV and $\sin\theta=0.01$, with the required value of 5×10^{-10} GeV for mediator-scalar DM coupling λ_3. Two other couplings, $\lambda_{\chi H}$ and λ_4, are found to have major roles in controlling the relic density. By varying the singlet scalar DM mass (inspired by Eq. (24)), we probe our parameter space in two classes: different values of $\lambda_{\chi H}$ and of λ_4 (see Fig. 1).

The behavior of the relic density $\Omega_\chi h^2$ regarding different Higgs-scalar DM couplings, $\lambda_{\chi H}$, is depicted in the logarithmic scale in Fig. 1(a). In addition to the fixed values of relevant parameters λ_3, m_{h_2} and $\sin\theta$, we have adopted $\lambda_{\chi H}$ as 10^{-12}, 5×10^{-13} and 10^{-13} as we fixed $\lambda_4 = 10^{-13}$. Through Fig. 1(a), it is obvious that the resonance occurs at $m_\chi \sim m_{h_2}/2$. For masses below the resonance, the relic density of the scalar component increases linearly in the log-scale, but for larger values ($m_\chi > m_{h_2}/2$) it seems that the relic density is indepen-

dent of the mass m_χ. The difference between these two regions is due to the process $h_2\to\chi\chi$ which is allowed in the region below the resonance.
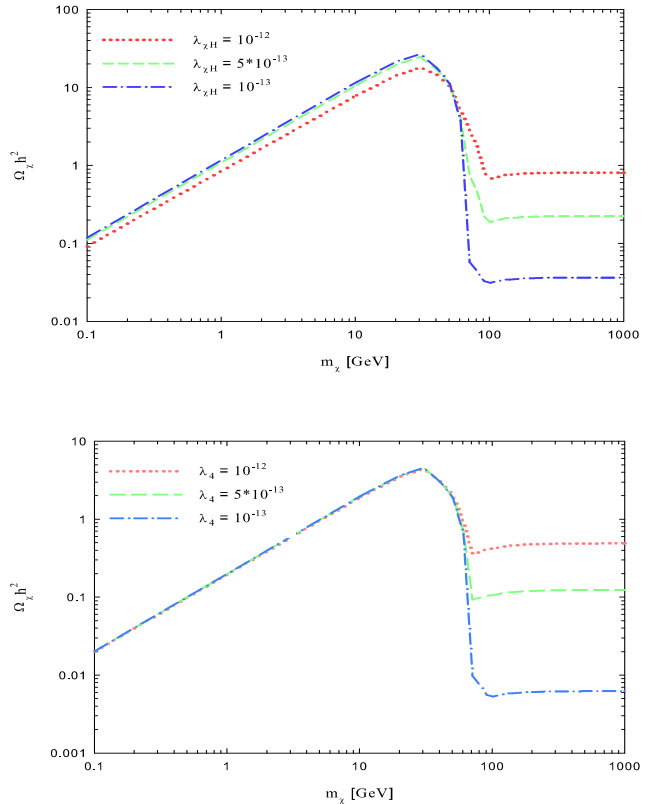

Fig. 1.   (color online) Relic density of scalar DM in terms of its mass. In this figure, we set $\lambda_3 = 5\times10^{-10}$, $m_{h_2} = 100$ GeV and $\sin\theta = 0.01$, a) for $\lambda_4 = 10^{-13}$ and different values of $\lambda_{\chi H}$, and b) for $\lambda_{\chi H} = 10^{-13}$ and different values of λ_4.
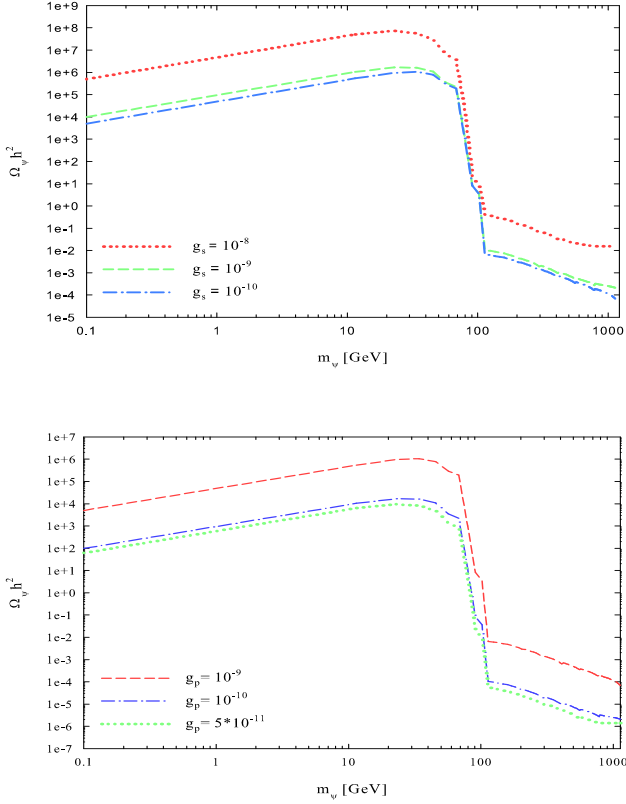
Fig. 2.   (color online) Relic density of the fermionic DM in terms of its mass. Other relevant parameters are taken as $m_{h_2}=100$ GeV and $\sin\theta=0.01$, a) for $g_p=10^{-9}$ and different values of g_s, and b) for $g_s=10^{-10}$ and different values of g_p.

The complementary analysis of the scalar component is plotted in Fig. 1(b), where we have chosen $\lambda_4=10^{-12}, 5\times10^{-13}$ and 10^{-13}. Regarding the resonance at $m_\chi \sim m_{h_2}/2$, as in Fig. 1(a), it can be seen that for the region below the resonance, the relic density grows when the scalar mass m_χ increases. This part of the graph seems to be independent of the λ_4-value and it is enhanced by the $h_2 \to \chi\chi$ process. After a significant drop at $m_\chi \sim m_{h_2}/2$, the relic density seems to be independent of DM mass for the region above the resonance. It is mainly influenced by changing the quartic coupling λ_4. Finishing our investigation of the scalar component, it should be noted that this analysis has a good overlap with a singlet scalar model [17]. We continue our investigation in parallel by turning our attention to the fermionic DM in the logarithmic scale, too. As before, we consider two classes of variations defined by the effect of scalar (parameterized by g_s) and pseudoscalar (parameterized by g_p) interactions of ψ (see Fig. 2). We first look at the coupling g_s so its best effects are formed for the values of 10^{-8}, 10^{-9} and 10^{-10} (Fig. 2(a)). Similar to the

scalar case, the resonance position occurs at $m_\psi \sim m_{h_2}/2$, so below this value one can observe the linear behavior of relic density which arises through the process $h_2 \to \psi\psi$. For $m_\psi > m_{h_2}/2$, the relic density changes by several order of magnitudes in a small interval of mass range. In this region, $\Omega_\psi h^2$ decreases when m_ψ increases. Note that the relic density is approximately independent of DM mass for large values of g_s. Also, for small enough values of g_s, decreasing g_s does not significantly change the relic density.

We keep on probing our model parameter space by choosing the appropriate values of g_p as 10^{-9}, 10^{-10} and 5×10^{-11}. In Fig. 2(b), we show the behavior of the relic density of the fermionic DM in terms of its mass. Here, there is a distinct point which should be expressed. As is seen, for very small values of g_p, the relic density is approximately independent of mass for massive DM. Similar to the scalar component, we can compare the fermionic component with models describing singlet fermionic DM like in Ref. [18].

4   Phenomenological implications

4.1   Direct searches

In this section, we search for signals inspired from XENON100 [43] and LUX [44] in spin-independent elastic scattering of DM off nuclei. Our intended process includes the fundamental interaction of DM-quark which occurs via the t-channel mediated by scalars h_1 and h_2. Taking into account the contribution of each DM component and using fractions $\xi_\psi = \frac{\Omega_\psi}{\Omega_{\text{DM}}}$ and $\xi_\chi = \frac{\Omega_\chi}{\Omega_{\text{DM}}}$, we investigate whether the model parameter space could be affected by the experimental results in this way. To this end, we calculate the following cross sections,

$$\sigma_{SI}^\psi = \xi_\psi \frac{g_s^2 \mu_m^2 \sin^2\theta \cos^2\theta}{\pi} \left(\frac{1}{m_{h_1}^2} - \frac{1}{m_{h_2}^2} \right)^2 \lambda_N^2, \qquad (25)$$

and

$$\sigma_{SI}^\chi = \xi_\chi \frac{\mu_m^2}{4\pi m_{h_1}^4 m_{h_2}^4 m_\chi^2} \Big[2v_H \lambda_{\chi H}(m_{h_1}^2 \sin^2\theta + m_{h_2}^2 \cos^2\theta),$$
$$+ \lambda_3 \sin2\theta(m_{h_1}^2 - m_{h_2}^2) \Big]^2 \lambda_N^2, \qquad (26)$$

where

$$\lambda_N = \frac{m_N}{v_H} \left[\sum_{q=u,d,s} f_q + \frac{2}{9}\left(1 - \sum_{q=u,d,s} f_q \right) \right] \approx 1.4\times10^{-3}. \quad (27)$$

Here, the parameter $\mu_m = \dfrac{m_N m_{\text{DM}}}{m_N + m_{\text{DM}}}$ is the reduced mass of DM-nucleon and $m_\chi = (m_{0\chi}^2 + \lambda_{\chi H} v_H^2)^{1/2}$ is the physical mass of the scalar DM. A cancellation effect [33] could occur when the two terms in Eq. (26) cancel each other out, giving a suppressed cross section which is not appropriate for our consideration. Generally, as was mentioned ear-

lier, a necessary condition for our DM candidates to be nonthermal is that they have extremely small couplings (g_s, $\lambda_{\chi H}$) which would yield cross sections out of the sensitivity of the aforementioned experiments by their established values of order $\sim 10^{-8}-10^{-12}$. Searching for other viable experiments, we consider the scattering of DM off free electrons in materials such as superconductors, semiconductors and graphene. From Ref. [45–47] it is seen that, although, these electron detectors are useful for light DM particles ($\mathcal{O}(\mathrm{MeV})$), the mediator mass should also be of order $\mathcal{O}(\mathrm{MeV})$, which is in conflict with the current model including $m_{h_2}=100$ GeV. For this reason, we are not able to probe such FIMP models directly. This outcome is consistent with the lack of direct experimental signals to date.

4.2 Indirect searches

4.2.1 Invisible Higgs decays

Since the ATLAS and CMS have recorded the signature of the SM Higgs [48, 49], new searches have been prepared for DM phenomenology. This is done by considering the branching ratios of the Higgs, especially for decaying into light DM candidates,

$$\mathrm{Br}(h_1 \rightarrow \mathrm{Invisible}) = \frac{\Gamma^{\mathrm{inv}}(h_1 \rightarrow \chi\chi) + \Gamma^{\mathrm{inv}}(h_1 \rightarrow \psi\psi)}{\Gamma^{\mathrm{SM}} + \Gamma^{\mathrm{inv}}}.$$

$$(28)$$

Regarding the experimental upper bound 0.23 for $\mathrm{Br}(h_1 \rightarrow \mathrm{Invisible})$ [50], we see that the decays of Higgs to both DM ψ and χ are suppressed due to small couplings g_s and g_p in the former case, and small λ_4 and $\lambda_{\chi H}$ in the latter. However, another constraint comes from the decay of our Higgs to h_2 (if kinematically possible, i.e. $m_{h_2} < m_{h_1}/2$) whose decay rate could be calculated as

$$\Gamma(h_1 \rightarrow h_2 h_2) = \frac{e_3^2}{8\pi m_{h_1}} \left(1 - \frac{4m_{h_2}^2}{m_{h_1}^2}\right)^{1/2} \Theta(m_{h_1} - 2m_{h_2}),$$

$$(29)$$

where e_3 is the relevant vertex factor which is presented in the Appendix, see Eq. (A11). From Eq. (29), it can be seen that for $\sin\theta = 0.01$ and $m_{h_1} = 125$ GeV, the result is sensitive to the choice of α_s. Consequently, we investigate the behavior of the aforementioned decay rate regarding the mass of the Higgs h_1 and the relevant coupling α_s. The parameter space of our Higgs sector is plotted in Figs. 3(a) and 3(b) where, respectively, we have calculated $\mathrm{Br}(h_1 \rightarrow h_2 h_2)$ as a function of m_{h_2} and depicted the parameter space for the (α_s, m_{h_2})-plane which is consistent with experimental measurements.

4.2.2 DM Self-Interactions

Of the different DM models, the collision-less cold DM (CDM) paradigm has been successful in explaining the large scale structure of the Universe. However, there are discrepancies between the CDM predictions and observations on smaller scales. The self-interacting DM
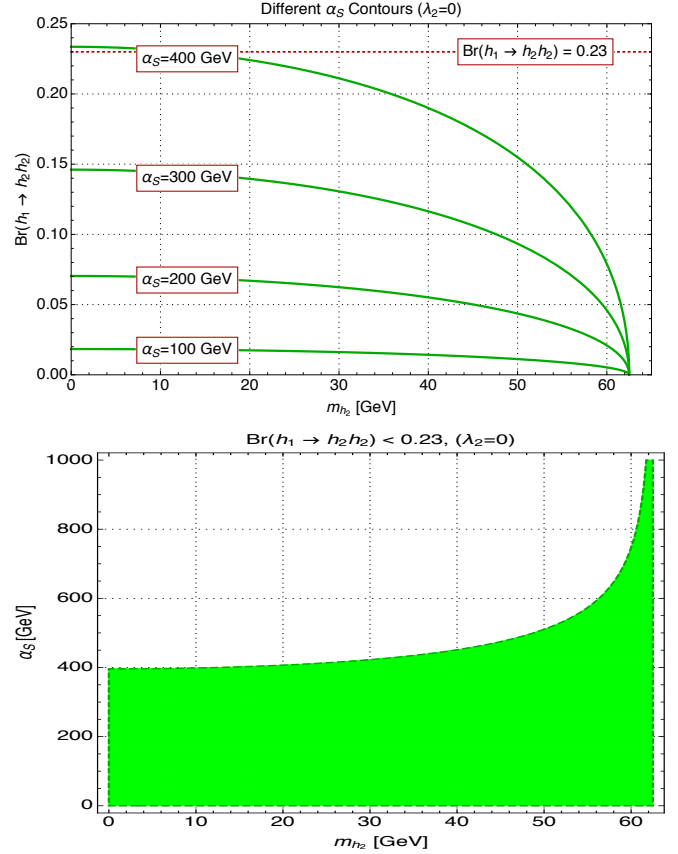

Fig. 3. (color online) a) Branching ratio of the SM Higgs to $h_2 h_2$ for different values of α_s and m_{h_2}. The red dashed line (at 0.23) is the experimental bound. b) The allowed region in the (α_s, m_{h_2})-parameter space where $\mathrm{Br}(h_1 \rightarrow h_2 h_2) < 0.23$. All points in the green area satisfy the perturbativity condition ($|e_3| < 4\pi$).

(SIDM) paradigm has the potential to solve these issues (for a review of SIDM, see Ref. [51]). Although such interactions cannot be detected in experiments, we can infer bounds on σ_{DM}/m by evaluating the trajectory of DM in colliding galaxy clusters [52, 53]. An updated work [54] has considered a set of twelve galaxies and six clusters in order to cover different scales. Including the core sizes from dwarf to cluster (varying from 0.5 to 50 kpc), the aforementioned cross section is parametrized as

$$\sigma_{\mathrm{DM}}/m \sim 0.1-2 \ \mathrm{cm}^2\mathrm{g}^{-1}. \tag{30}$$

In this section, we analyze this constraint to see if it can put new limits on the parameter space of our model.

The DM self-interaction in the present model includes the processes $\chi\chi \rightarrow \chi\chi$, $\psi\psi \rightarrow \psi\psi$, $\chi\chi \rightarrow \psi\psi$, $\psi\psi \rightarrow \chi\chi$ and $\chi\psi \rightarrow \chi\psi$. Except for $\chi\chi \rightarrow \chi\chi$ and $\psi\psi \rightarrow \psi\psi$, the processes contain cross sections proportional to the coupling λ_4, which is very small in our work. Therefore,

the specified processes do not contribute to this cosmological constraint. Concerning the processes $\chi\chi \to \chi\chi$ and $\psi\psi \to \psi\psi$, we start first with the scalar component which has been studied in a singlet FIMP scalar model in Ref. [55]. Here, we just consider the contact interaction which is parameterized by the coupling λ_χ. Practically, we neglect the contributions from the s-channel mediated diagrams. This is due to the small couplings of the scalar DM with both the SM Higgs and the mediator and also due to the large masses which appear in the propagator. One way to vitalize the s-channel contribution might be through fine tuning by considering the scattering near resonance (similar to Ref. [55]). In this way, in the denominator of the propagator, m_{h_2} should be tuned such that $|m_\chi - m_{h_2}| \ll 1$ GeV. Considering the values of couplings needed for the observed relic density, this scenario fails too. Therefore, following Ref. [55], we obtain the self-interaction cross section per mass m_χ, as

$$\frac{\sigma_\chi}{m_\chi} = \frac{9\lambda_\chi^2}{2\pi m_\chi^3}, \quad (31)$$

where λ_χ is the quartic self-coupling of the scalar DM (see Eq. (2)). Following the theoretical constraints in Eqs. (7) and (8), we obtain an experimental upper bound of about 0.1 GeV on the mass of the scalar DM, which is depicted in Fig. 4. Going back to Figs. 1(a) and 1(b), we observe that this range of scalar mass can produce proper total relic density along with the contribution of the fermionic component.
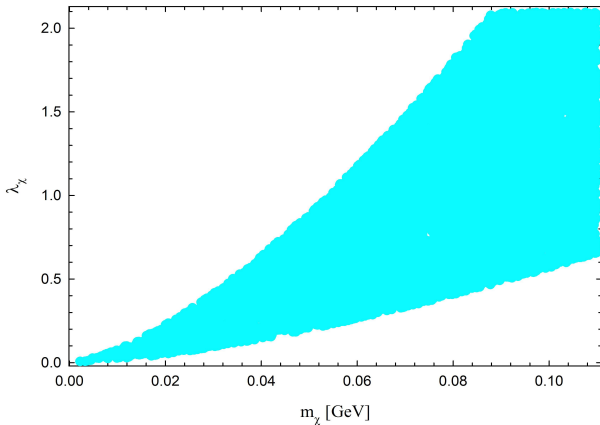

Fig. 4. (color online) The colored area depicts the ranges of parameter space in the (m_χ, λ_χ)-plane for the scalar DM self-interaction cross section in the range 0.1-2 cm^{2}g^{-1}.

Another significant point, which we would like to clarify in this work, is the self-interaction of a singlet fermionic FIMP DM. In general, we have two concerns. First, it should be noted that significant self-scattering at dwarf scales requires the mediator masses to be smaller than 100 MeV [56]. In fact, following Ref. [56], the fermionic DM should satisfy the relation $(m_\psi/10 \text{ GeV})(m_{h_2}/100 \text{ MeV})^2 \sim 1$, with Yukawa interactions of strengths 10^{-5} to 1, which is in contradiction with our fermionic DM coupling and mediator mass. Second, if the mediator couples to the SM through a Higgs portal, one should make sure that the mediator decays before the start of Big Bang nucleosynthesis (BBN), so the decay products do not affect the BBN. Eventually, we require a mediator with a lifetime $\sim$1 s. One way to alleviate the second constraint in DM models with extremely weak interactions is to open a new decay channel for the mediator so it can decay faster. This is done in Refs. [57] and [58] by coupling the mediator to a light sterile neutrino (it should be noted that this new coupling does not affect the relic density). However, the first constraint (light mediator) is in conflict with our mediator of mass 100 GeV (and other usual two-component models). A promising solution seems to be to work at the resonance region to minimize this mass constraint [59]. Due to the small coupling g_p (pseudoscalar interaction type), and the fact that there is an energy (velocity) dependent correction to the width in the resonance region (as explained in Ref. [59]), we conclude that the resonance DM self-interaction scenario does not work in fermionic FIMP models.

5   Conclusions and outlook

We have constructed a minimal two-component model to analyze the implications of multi-component DM in the Universe. Using the freeze-in mechanism, we calculated the relic abundance predicted by our model and compared it to the observed relic abundance of DM. We started our investigation by proposing two DM particles: a real scalar and a Dirac fermion. Furthermore, a scalar mediator between the dark sector and the SM sector was added. The couplings for this interaction are assumed to be small as we are utilizing the freeze-in mechanism. We solved two independent Boltzmann equations in order to obtain the observed relic density with the contributions of both DM components. It should be noted here that at the time of finishing this work, a new version of micrOMEGAs [60] was presented which can compute the relic abundance of FIMP candidates. In the following, using theoretical constraints, we probed the model parameter space and compared our results with the relevant singlet models. Although it is difficult to probe FIMP particles, we looked for astrophysical probes, first considering direct detection. We considered the scattering of DM particles off nuclei and free electrons. As we explained, it is impossible to see this direct signature for our FIMP model.

In order to constrain the parameter space of our model, we also checked the limits from the invisible decay width of the Higgs. Finally, we probed the self-interaction of DM in this model. We used the bounds on non-gravitational interactions of DM in giant cluster collisions and constrained the mass of DM candidates in our model. In addition to the mentioned probes of DM, we can refer to the Big Bang nucleosynthesis and cosmic microwave background constraints regarding dark photons and dark Higgs [61, 62]. These neutral bosons mix with the SM photon (kinetically) and the SM Higgs, respectively, by accepting significant bounds on their coupling parameters.

Two-component DM is a starting point for considering multi-component configurations where DM consists of various types of fundamental particles (scalar, fermion, vector and etc). The freeze-in framework is also a well-motivated approach which may be probed more extensively by future experiments.

Appendix A

DM production cross sections and decay rates

Here, we present our calculation of the fermionic DM production cross-sections which contribute to the relic density of our model:

$$(\sigma v_{\rm rel})_{\overline{f}f \to \overline{\psi}\psi} = \frac{s\sin^2 2\theta}{32\pi} N_c \left(\frac{m_f}{v_H}\right)^2 \left(1 - \frac{4m_f^2}{s}\right) F, \tag{A1}$$

$$(\sigma v_{\rm rel})_{ZZ \to \overline{\psi}\psi} = \frac{\sin^2 2\theta}{36\pi} \left(\frac{m_Z^2}{v_H}\right)^2 \left(2 + \frac{(s-2m_Z^2)^2}{4m_Z^4}\right) F, \tag{A2}$$

$$(\sigma v_{\rm rel})_{W^+W^- \to \overline{\psi}\psi} = \frac{\sin^2 2\theta}{36\pi} \left(\frac{m_W^2}{v_H}\right)^2 \left(2 + \frac{(s-2m_W^2)^2}{4m_W^4}\right) F, \tag{A3}$$

where

$$F = \left(1 - \frac{4m_\psi^2}{s}\right)^{3/2} \left(g_\psi^2 + \frac{sg_p^2}{s-4m_\psi^2}\right) \left\{\frac{1}{(s-m_{h_1}^2)^2 + m_{h_1}^2 \Gamma_{h_1}^2} + \frac{1}{(s-m_{h_2}^2)^2 + m_{h_2}^2 \Gamma_{h_2}^2} - \frac{2(s-m_{h_1}^2)(s-m_{h_2}^2) + 2m_{h_1}m_{h_2}\Gamma_{h_1}\Gamma_{h_2}}{[(s-m_{h_1}^2)^2 + m_{h_1}^2 \Gamma_{h_1}^2][(s-m_{h_2}^2)^2 + m_{h_2}^2 \Gamma_{h_2}^2]}\right\}. \tag{A4}$$

$$
\begin{aligned}
(\sigma v_{\rm rel})_{h_1 h_1 \to \overline{\psi}\psi} = {} & \frac{1}{4\pi s}\left(1 - \frac{4m_\psi^2}{s}\right)^{1/2} \left\{(g_p^2 s + g_\psi^2(s-4m_\psi^2))\left[\frac{e_1^2 \sin^2\theta}{(s-m_{h_1}^2)^2 + m_{h_1}^2 \Gamma_{h_1}^2} + \frac{e_2^2\cos^2\theta}{(s-m_{h_2}^2)^2 + m_{h_2}^2 \Gamma_{h_2}^2}\right.\right. \\[2mm]
& + \left.\frac{e_1 e_2 \sin 2\theta((s-m_{h_1}^2)(s-m_{h_2}^2) + m_{h_1}m_{h_2}\Gamma_{h_1}\Gamma_{h_2})}{((s-m_{h_1}^2)^2 + m_{h_1}^2 \Gamma_{h_1}^2)((s-m_{h_2}^2)^2 + m_{h_2}^2 \Gamma_{h_2}^2)}\right] - 8m_\psi g_\psi \sin^2\theta\left[\frac{e_1\sin\theta(s-m_{h_1}^2)}{(s-m_{h_1}^2)^2 + m_{h_1}^2 \Gamma_{h_1}^2} + \frac{e_2\cos\theta(s-m_{h_2}^2)}{(s-m_{h_2}^2)^2 + m_{h_2}^2 \Gamma_{h_2}^2}\right] \\[2mm]
& \times \left[\frac{\mathrm{arctanh}(x_1)[g_p^2(2m_{h_1}^2 - 3s) - g_\psi^2(2m_{h_1}^2 - 8m_\psi^2 + s)]}{x_1(s-2m_{h_1})} + g_p^2 - g_\psi^2\right] \\[2mm]
& - 4\sin^4\theta\left[g_p^4 + g_\psi^4 - 2g_p^2 g_\psi^2 + \frac{(m_{h_1}^2(g_p^2 - g_\psi^2) + 4g_\psi^2 m_\psi^2)^2 - 8g_p^2 g_\psi^2 m_\psi^2 s}{m_{h_1}^4 + m_\psi^2(s-4m_{h_1}^2)}\right. \\[2mm]
& - \frac{\mathrm{arctanh}(x_1)}{x_1(s-2m_{h_1}^2)}\left(g_p^4[6m_{h_1}^4 + s(s-4m_{h_1}^2)] - 2g_p^2 g_\psi^2[2m_{h_1}^2(3m_{h_1}^2 - 4m_\psi^2) + s(s-4m_{h_1}^2)]\right. \\[2mm]
& + \left.\left.\left.g_\psi^4[2m_{h_1}^2(3m_{h_1}^2 - 8m_\psi^2) + s(s-4m_{h_1}^2) + 16m_\psi^2(s-2m_\psi^2)]\right)\right]\right\},
\end{aligned}\tag{A5}
$$

$$
\begin{aligned}
(\sigma v_{\rm rel})_{h_2 h_2 \to \overline{\psi}\psi} =\ & \frac{1}{4\pi s}\left(1-\frac{4m_\psi^2}{s}\right)^{1/2}\times\Bigg\{(g_p^2 s+g_\psi^2(s-4m_\psi^2))\left[\frac{e_3^2\sin^2\theta}{(s-m_{h_1}^2)^2+m_{h_1}^2\Gamma_{h_1}^2}+\frac{e_4^2\cos^2\theta}{(s-m_{h_2}^2)^2+m_{h_2}^2\Gamma_{h_2}^2}\right.\\
& +\left.\frac{e_3 e_4\sin2\theta[(s-m_{h_1}^2)(s-m_{h_2}^2)+m_{h_1}m_{h_2}\Gamma_{h_1}\Gamma_{h_2}]}{[(s-m_{h_1}^2)^2+m_{h_1}^2\Gamma_{h_1}^2][(s-m_{h_2}^2)^2+m_{h_2}^2\Gamma_{h_2}^2]}\right]-8m_\psi g_\psi\cos^2\theta\left[\frac{e_3\sin\theta(s-m_{h_1}^2)}{(s-m_{h_1}^2)^2+m_{h_1}^2\Gamma_{h_1}^2}+\frac{e_4\cos\theta(s-m_{h_2}^2)}{(s-m_{h_2}^2)^2+m_{h_2}^2\Gamma_{h_2}^2}\right]\\
& \times\left[\frac{\operatorname{arctanh}(x_2)[g_p^2(2m_{h_2}^2-3s)-g_\psi^2(2m_{h_2}^2-8m_\psi^2+s)]}{x_2(s-2m_{h_2})}+g_p^2-g_\psi^2\right]\\
& -4\cos^4\theta\left[g_p^4+g_\psi^4-2g_p^2 g_\psi^2+\frac{(m_{h_2}^2(g_p^2-g_\psi^2)+4g_\psi^2 m_\psi^2)^2-8g_p^2 g_\psi^2 m_\psi^2 s}{2m_{h_2}^4+2m_\psi^2(s-4m_{h_2}^2)}\right.\\
& -\frac{\operatorname{arctanh}(x_2)}{x_2(s-2m_{h_2})^2}\left(g_p^4\left(6m_{h_2}^4+s(s-4m_\psi^2)\right)-2g_p^2 g_\psi^2\left(2m_{h_2}^2(3m_{h_2}^2-4m_\psi^2)+s(s-4m_\psi^2)\right)\right.\\
& +\left.\left.g_\psi^4\left(2m_{h_2}^2(3m_{h_2}^2-8m_\psi^2)+s(s-4m_\psi^2)+16m_\psi^2(s-2m_{h_2}^2)\right)\right)\right]\Bigg\},
\end{aligned}
\tag{A6}
$$

$$
\begin{aligned}
(\sigma v_{\rm rel})_{h_1 h_2 \to \overline{\psi}\psi} =\ & \frac{1}{4\pi s}\left(1-\frac{4m_\psi^2}{s}\right)^{1/2}\Bigg\{[g_p^2 s+g_\psi^2(s-4m_\psi^2)]\left[\frac{e_2^2\sin^2\theta}{(s-m_{h_1}^2)^2+m_{h_1}^2\Gamma_{h_1}^2}+\frac{e_3^2\cos^2\theta}{(s-m_{h_2}^2)^2+m_{h_2}^2\Gamma_{h_2}^2}\right.\\
& +\left.\frac{e_2 e_3\sin2\theta((s-m_{h_1}^2)(s-m_{h_2}^2)+m_{h_1}m_{h_2}\Gamma_{h_1}\Gamma_{h_2})}{[(s-m_{h_1}^2)^2+m_{h_1}^2\Gamma_{h_1}^2][(s-m_{h_2}^2)^2+m_{h_2}^2\Gamma_{h_2}^2]}\right]-4m_\psi g_\psi\sin2\theta\left[\frac{e_2\sin\theta(s-m_{h_1}^2)}{(s-m_{h_1}^2)^2+m_{h_1}^2\Gamma_{h_1}^2}+\frac{e_3\cos\theta(s-m_{h_2}^2)}{(s-m_{h_2}^2)^2+m_{h_2}^2\Gamma_{h_2}^2}\right]\\
& \times\left[\frac{\operatorname{arctanh}(x_i)}{x_i(s-2m_{h_i}^2)}[g_p^2(m_{h_1}^2+m_{h_2}^2-3s)-g_\psi^2(m_{h_1}^2+m_{h_2}^2-8m_\psi^2+s)]+g_p^2-g_\psi^2\right]\\
& -\sin^2 2\theta\left[\frac{1}{2m_{h_i}^4+2m_\psi^2(s-4m_{h_i}^2)}\left(-g_p^4[2m_{h_i}^4+m_{h_i}^2(m_{h_j}^2-8m_\psi^2)+2m_\psi^2 s]\right.\right.\\
& +2g_p^2 g_\psi^2\left(2m_{h_i}^4+m_{h_i}^2(m_{h_j}^2-10m_\psi^2)-2m_\psi^2(m_{h_j}^2-3s)\right)\Big)-g_\psi^4[(m_{h_i}^2-4m_\psi^2)(2m_{h_i}^2+m_{h_j}^2-4m_\psi^2)-2m_\psi^2 s]\\
& +\frac{\operatorname{arctanh}(x_i)}{x_i(s-2m_{h_i})^2}\left(g_p^4[3m_{h_i}^2+m_{h_i}^2(4m_{h_j}^2-3s)-m_{h_j}^4-m_{h_i}^2 s+s^2]\right.\\
& +2g_p^2 g_\psi^2[-3m_{h_i}^2+m_{h_i}^2(3(4m_\psi^2+s)-4m_{h_j}^2)+m_{h_j}^4+m_{h_j}^2(s-4m_\psi^2)-s^2]\\
& +\left.\left.\left.g_\psi^4[3m_{h_i}^2+m_{h_i}^2(-3(8m_\psi^2+s)+4m_{h_j}^2)-m_{h_j}^4-m_{h_j}^2(s-8m_\psi^2)+s^2+16m_\psi^2(s-2m_\psi^2)]\right)\right]\right]\Bigg\},
\end{aligned}
\tag{A7}
$$

where the auxiliary parameters and coupling constants have the following expressions

$$
x_i=\frac{(s-4m_\psi^2)^{\frac{1}{2}}(s-4m_{h_i}^2)^{\frac{1}{2}}}{(s-2m_{h_i}^2)},\quad\text{with}\quad i,j=1,2\ \text{and}\ i\neq j,
\tag{A8}
$$

$$
e_1=-\sin^2\theta(\alpha_s\sin\theta+6v_H\lambda_2\cos\theta)-3\cos^2\theta(\lambda_1\sin\theta+2v_H\lambda_H\cos\theta),
\tag{A9}
$$

$$
e_2=\sin2\theta(-\frac{1}{2}\alpha_s\sin\theta+3\lambda_H v_H\cos\theta)-\lambda_1\cos\theta(1-3\sin^2\theta)+2v_H\lambda_2\sin\theta(1-3\cos^2\theta),
\tag{A10}
$$

$$
e_3=\sin2\theta(-\frac{1}{2}\alpha_s\cos\theta-3\lambda_H v_H\sin\theta)-\lambda_1\sin\theta(1-3\cos^2\theta)-2v_H\lambda_2\cos\theta(1-3\sin^2\theta),
\tag{A11}
$$

$$
e_4=-\cos^2\theta(\alpha_s\cos\theta-6v_H\lambda_2\sin\theta)-3\sin^2\theta(\lambda_1\cos\theta-2v_H\lambda_H\sin\theta).
\tag{A12}
$$

The scalar component will account for the DM phenomenology by the following annihilation cross sections:

$$
(\sigma v_{\rm rel})_{\bar{f}f\to\chi\chi}=\frac{1}{16\pi}\left(\frac{m_f}{v_H}\right)^2\left(1-\frac{4m_f^2}{s}\right)^{3/2}N_c R,
\tag{A13}
$$

$$
(\sigma v_{\rm rel})_{ZZ\to\chi\chi}=\frac{1}{36\pi s}\left(\frac{m_Z^2}{v_H}\right)^2\left(2+\frac{(s-2m_Z^2)^2}{4m_Z^4}\right)\left(1-\frac{4m_Z^2}{s}\right)^{1/2}R,
\tag{A14}
$$

$$(\sigma v_{\rm rel})_{W^+W^-\to\chi\chi} = \frac{1}{36\pi s}\left(\frac{m_W^2}{v_H}\right)^2\left(2+\frac{(s-2m_W^2)^2}{4m_W^4}\right)\left(1-\frac{4m_W^2}{s}\right)^{1/2}R \tag{A15}$$

where

$$R = \frac{e_5^2\cos^2\theta}{(s-m_{h_1}^2)^2+m_{h_1}^2\Gamma_{h_1}^2}+\frac{e_6^2\sin^2\theta}{(s-m_{h_2}^2)^2+m_{h_2}^2\Gamma_{h_2}^2}-\frac{e_5e_6\sin2\theta[(s-m_{h_1}^2)(s-m_{h_2}^2)+m_{h_1}m_{h_2}\Gamma_{h_1}\Gamma_{h_2}]}{[(s-m_{h_1}^2)^2+m_{h_1}^2\Gamma_{h_1}^2][(s-m_{h_2}^2)^2+m_{h_2}^2\Gamma_{h_2}^2]}. \tag{A16}$$

$$\begin{aligned}(\sigma v_{\rm rel})_{h_1h_1\to\chi\chi} = \frac{1}{16\pi s}\left(1-\frac{4m_{h_1}^2}{s}\right)^{1/2}&\left\{\left[\frac{e_1^2e_5^2}{(s-m_{h_1}^2)^2+m_{h_1}^2\Gamma_{h_1}^2}+\frac{e_2^2e_6^2}{(s-m_{h_2}^2)^2+m_{h_2}^2\Gamma_{h_2}^2}\right.\right.\\&+\frac{2e_1e_2e_5e_6[(s-m_{h_1}^2)(s-m_{h_2}^2)+m_{h_1}m_{h_2}\Gamma_{h_1}\Gamma_{h_2}]}{[(s-m_{h_1}^2)^2+m_{h_1}^2\Gamma_{h_1}^2][(s-m_{h_2}^2)^2+m_{h_2}^2\Gamma_{h_2}^2]}\bigg]\\&-\left(\frac{8e_5^2}{s-2m_{h_1}^2}F(y_1)+2e_7\right)\left[\frac{e_1e_5(s-m_{h_1}^2)}{(s-m_{h_1}^2)^2+m_{h_1}^2\Gamma_{h_1}^2}+\frac{e_2e_6(s-m_{h_2}^2)}{(s-m_{h_2}^2)^2+m_{h_2}^2\Gamma_{h_2}^2}\right]\\&+\frac{8e_5^2}{s-2m_{h_1}^2}F(y_1)\left[\frac{e_5^2}{s-2m_{h_1}^2}\left[\frac{1}{F(y_1)(1-y_1^2)}+1\right]+e_7\right]+e_7^2\bigg\},\end{aligned} \tag{A17}$$

$$\begin{aligned}(\sigma v_{\rm rel})_{h_2h_2\to\chi\chi} = \frac{1}{16\pi s}\left(1-\frac{4m_{h_2}^2}{s}\right)^{1/2}&\left\{\left[\frac{e_3^2e_5^2}{(s-m_{h_1}^2)^2+m_{h_1}^2\Gamma_{h_1}^2}+\frac{e_4^2e_6^2}{(s-m_{h_2}^2)^2+m_{h_2}^2\Gamma_{h_2}^2}\right.\right.\\&+\frac{2e_3e_4e_5e_6[(s-m_{h_1}^2)(s-m_{h_2}^2)+m_{h_1}m_{h_2}\Gamma_{h_1}\Gamma_{h_2}]}{[(s-m_{h_1}^2)^2+m_{h_1}^2\Gamma_{h_1}^2][(s-m_{h_2}^2)^2+m_{h_2}^2\Gamma_{h_2}^2]}\bigg]\\&-\left(\frac{8e_6^2}{s-2m_{h_2}^2}F(y_2)+2e_8\right)\left[\frac{e_3e_5(s-m_{h_1}^2)}{(s-m_{h_1}^2)^2+m_{h_1}^2\Gamma_{h_1}^2}+\frac{e_4e_6(s-m_{h_2}^2)}{(s-m_{h_2}^2)^2+m_{h_2}^2\Gamma_{h_2}^2}\right]\\&+\frac{8e_6^2}{s-2m_{h_2}^2}F(y_2)\left[\frac{e_6^2}{s-2m_{h_2}^2}(\frac{1}{F(y_2)(1-y_2^2)}+1)+e_8\right]+e_8^2\bigg\},\end{aligned} \tag{A18}$$

$$\begin{aligned}(\sigma v_{\rm rel})_{h_1h_2\to\chi\chi} = \frac{1}{16\pi s}\left(1-\frac{4m_{h_i}^2}{s}\right)^{1/2}&\left\{\left[\frac{e_2^2e_5^2}{(s-m_{h_1}^2)^2+m_{h_1}^2\Gamma_{h_1}^2}+\frac{e_3^2e_6^2}{(s-m_{h_2}^2)^2+m_{h_2}^2\Gamma_{h_2}^2}\right.\right.\\&+\frac{2e_2e_3e_5e_6[(s-m_{h_1}^2)(s-m_{h_2}^2)+m_{h_1}m_{h_2}\Gamma_{h_1}\Gamma_{h_2}]}{[(s-m_{h_1}^2)^2+m_{h_1}^2\Gamma_{h_1}^2][(s-m_{h_2}^2)^2+m_{h_2}^2\Gamma_{h_2}^2]}\bigg]\\&-\left(\frac{8e_5e_6}{s-2m_{h_i}^2}F(y_i)+2e_9\right)\left[\frac{e_2e_5(s-m_{h_1}^2)}{(s-m_{h_1}^2)^2+m_{h_1}^2\Gamma_{h_1}^2}+\frac{e_3e_6(s-m_{h_2}^2)}{(s-m_{h_2}^2)^2+m_{h_2}^2\Gamma_{h_2}^2}\right]\\&+\frac{8e_5e_6}{s-2m_{h_i}^2}F(y_i)\left[\frac{e_5e_6}{s-2m_{h_i}^2}(\frac{1}{F(y_i)(1-y_i^2)}+1)+e_9\right]+e_9^2\bigg\},\end{aligned} \tag{A19}$$

where we have employed parameter y_i and function $F(y_i)$ as

$$y_i = \frac{(s-4m_\chi^2)^{\frac{1}{2}}(s-4m_{h_i}^2)^{\frac{1}{2}}}{(s-2m_{h_i}^2)}$$

$$F(y_i) = \frac{1}{y_i}{\rm arctanh}(y_i) \qquad {\rm with}\ \ i=1,2, \tag{A20}$$

and also for coupling constants, we have the following parameters:

$$e_5=-[v_H\lambda_{\chi H}\cos\theta+\lambda_3\sin\theta]\times2!, \tag{A21}$$

$$e_6=[v_H\lambda_{\chi H}\sin\theta-\lambda_3\cos\theta]\times2!, \tag{A22}$$

$$e_7=-[\frac{1}{2}\lambda_{\chi H}\cos^2\theta+\lambda_4\sin^2\theta]\times4!, \tag{A23}$$

$$e_8=-[\frac{1}{2}\lambda_{\chi H}\sin^2\theta+\lambda_4\cos^2\theta]\times4!, \tag{A24}$$

$$e_9=\left[\left(\frac{1}{2}\lambda_{\chi H}-\lambda_4\right)\sin2\theta\right]\times2!. \tag{A25}$$

Finally, the decay rates of scalars h_i (with $i=1,2$) into fermionic and scalar DM particles are given as:

$$\Gamma(h_i\to\bar{\psi}\psi)=\frac{S_i^2\theta}{8\pi}(1-4m_\psi^2/m_{h_i}^2)^{\frac{3}{2}}\left[g_\psi^2+\frac{m_{h_i}^2g_p^2}{m_{h_i}^2-4m_\psi^2}\right] \tag{A26}$$

$$\Gamma(h_1\to\chi\chi)=\frac{e_5^2}{32\pi m_{h_1}}(1-4m_\chi^2/m_{h_1}^2)^{\frac{1}{2}}, \tag{A27}$$

$$\Gamma(h_2\to\chi\chi)=\frac{e_6^2}{32\pi m_{h_2}}(1-4m_\chi^2/m_{h_2}^2)^{\frac{1}{2}}, \tag{A28}$$

where we have defined $S_1\theta=\sin\theta$ and $S_2\theta=\cos\theta$.

References

1 P. Gondolo, and G. Gelmini, Nucl. Phys. B, **360**: 145 (1991)
2 M. Srednicki, R. Watkins, and K. A. Olive, Nucl. Phys. B, **310**: 693 (1988)
3 H. Y. Chiu, Phys. Rev. Lett., **17**: 712 (1966)
4 G. Jungman, M. Kamionkowski, and K. Griest, Phys. Rept., **267**: 195 (1996)
5 H. C. Cheng, J. L. Feng, and K. T. Matchev, Phys. Rev. Lett., **89**: 211301 (2002)
6 G. Servant, and T. M. P. Tait, Nucl. Phys. B, **650**: 391 (2003)
7 V. Silveira, and A. Zee, Phys. Lett. B, **161**: 136 (1985)
8 J. McDonald, Phys. Rev. D, **50**: 3637 (1994)
9 C. P. Burgess, M. Pospelov, and T. ter Veldhuis, Nucl. Phys. B, **619**: 709 (2001)
10 V. Barger, P. Langacker, M. McCaskey et al, Phys. Rev. D, **77**: 035005 (2008)
11 Y. G. Kim, K. Y. Lee, and S. Shin, JHEP, **0805**: 100 (2008)
12 M. M. Ettefaghi and R. Moazzemi, JCAP, **1302**: 048 (2013)
13 M. Fairbairn and R. Hogan, JHEP, **1309**: 022 (2013)
14 J. McDonald, Phys. Rev. Lett., **88**: 091304 (2002)
15 L. J. Hall, K. Jedamzik, J. March-Russell, and S. M. West, JHEP, **1003**: 080 (2010)
16 N. Bernal, M. Heikinheimo, T. Tenkanen, K. Tuominen, and V. Vaskonen, Int. J. Mod. Phys. A, **32**(27): 1730023 (2017) doi: 10.1142/S0217751X1730023X [arXiv:1706.07442 [hep-ph]]
17 C. E. Yaguna, JHEP, **1108**: 060 (2011)
18 M. Klasen and C. E. Yaguna, JCAP, **1311**: 039 (2013)
19 S. Yaser Ayazi, S. M. Firouzabadi, and S. P. Zakeri, J. Phys. G, **43**(9): 095006 (2016)
20 A. Merle and A. Schneider, Phys. Lett. B, **749**: 283 (2015)
21 A. Merle and M. Totzauer, JCAP, **1506**: 011 (2015)
22 B. Shakya, Mod. Phys. Lett. A, **31**(06): 1630005 (2016)
23 Z. Kang, Eur. Phys. J. C, **75**(10): 471 (2015) doi:10.1140/epjc/s10052-015-3702-4 [arXiv:1411.2773 [hep-ph]]
24 A. Biswas and A. Gupta, JCAP, **1609**: 044 (2016)
25 M. Pandey, D. Majumdar, and K. P. Modak, arXiv: hepph/1709.05955
26 P. S. Bhupal Dev, A. Mazumdar, and S. Qutub, Front. in Phys., **2**: 26 (2014) doi:10.3389/fphy.2014.00026 [arXiv:1311.5297 [hep-ph]]
27 S. Profumo, K. Sigurdson, and L. Ubaldi, JCAP, **0912**: 016 (2009)
28 G. B. Gelmini, Nucl. Phys. Proc. Suppl, **138**: 32 (2005)
29 G. Duda, G. Gelmini, P. Gondolo et al, Phys. Rev. D, **67**: 023505 (2003)
30 G. Duda, G. Gelmini, and P. Gondolo, Phys. Lett. B, **529**: 187 (2002)
31 J. Herrero-Garcia, A. Scaffidi, M. White et al, JCAP, **1711**: 021 (2017)
32 A. Biswas, D. Majumdar, and P. Roy, JHEP, **1504**: 065 (2015)
33 S. Esch, M. Klasen, and C. E. Yaguna, JHEP, **1409**: 108 (2014)
34 S. Bhattacharya, A. Drozd, B. Grzadkowski et al, JHEP, **1310**: 158 (2013)
35 A. Biswas, D. Majumdar, A. Sil et al, JCAP, **1312**: 049 (2013)
36 D. Chialva, P. S. B. Dev, and A. Mazumdar, Phys. Rev. D, **87**(6): 063522 (2013) doi:10.1103/PhysRevD.87.063522 [arXiv:1211.0250 [hep-ph]]
37 A. Dutta Banik, M. Pandey, D. Majumdar et al, Eur. Phys. J. C, **77**(10): 657 (2017)
38 K. P. Modak, JHEP, **1503**: 064 (2015)
39 K. S. Babu, and R. N. Mohapatra, Phys. Rev. D, **89**: 115011 (2014)
40 P. A. R. Ade et al (Planck Collaboration), Astron. Astrophys, **571**: A31 (2014)
41 E. W. Kolb and M. S. Turner, Front. Phys., **69**: 1 (1990)
42 J. Edsjo and P. Gondolo, Phys. Rev. D, **56**: 1879 (1997)
43 E. Aprile et al (XENON100 Collaboration), Phys. Rev. Lett., **109**: 181301 (2012)
44 D. S. Akerib et al (LUX Collaboration), Phys. Rev. Lett., **112**: 091303 (2014)
45 Y. Hochberg, Y. Zhao, and K. M. Zurek, Phys. Rev. Lett., **116**(1): 011301 (2016)
46 Y. Hochberg, M. Pyle, Y. Zhao et al, JHEP, **1608**: 057 (2016)
47 Y. Hochberg, Y. Kahn, M. Lisanti et al, Phys. Lett. B, **772**: 239 (2017)
48 G. Aad et al (ATLAS Collaboration), Phys. Lett. B, **716**: 1 (2012)
49 S. Chatrchyan et al (CMS Collaboration), Phys. Lett. B, **716**: 30 (2012)
50 G. Belanger, B. Dumont, U. Ellwanger et al, Phys. Lett. B, **723**: 340 (2013)
51 S. Tulin, and H. B. Yu, arXiv: hepph/1705.02358
52 D. Clowe, A. Gonzalez, and M. Markevitch, Astrophys. J, **604**: 596 (2004)
53 S. W. Randall, M. Markevitch, D. Clowe et al, Astrophys. J, **679**: 1173 (2008)
54 M. Kaplinghat, S. Tulin, and H. B. Yu, Phys. Rev. Lett., **116**(4): 041302 (2016)
55 R. Campbell, S. Godfrey, H. E. Logan et al, Phys. Rev. D, **92**(5): 055031 (2015)
56 S. Tulin, H. B. Yu, and K. M. Zurek, Phys. Rev. D, **87**(11): 115007 (2013)
57 K. Kainulainen, K. Tuominen, and V. Vaskonen, Phys. Rev. D, **93**(1): 015016 (2016); Phys. Rev. D, **95**(7): 079901 (2017)
58 C. Kouvaris, I. M. Shoemaker, and K. Tuominen, Phys. Rev. D, **91**(4): 043519 (2015)
59 M. Duch, and B. Grzadkowski, JHEP, **1709**: 159 (2017)
60 G. Blanger, F. Boudjema, A. Goudelis et al, arXiv: hepph/1801.03509
61 A. Fradette, M. Pospelov, J. Pradler, and A. Ritz, Phys. Rev. D, **90**(3): 035022 (2014)
62 J. Berger, K. Jedamzik, and D. G. E. Walker, JCAP, **1611**: 032 (2016)